Space Weather

RESEARCH ARTICLE
10.1029/2024SW004095

Radiation Exposure and Shielding Effects on the Lunar Surface

Daniel Matthiä[1] **and Thomas Berger**[1]

[1]German Aerospace Center (DLR), Institute of Aerospace Medicine, Cologne, Germany

Abstract The Moon will be a primary target for human space exploration in the near future. A limiting factor for a crewed mission to the Moon is the radiation dose during their stay on the lunar surface. While the total dose is expected to be dominated by the galactic cosmic radiation (GCR), the potential occurrence of large solar energetic particle events may lead to severe short-term effects and endanger the success of the mission. This work investigated the expected dose rates for maximum GCR intensity and the total dose from several historical solar energetic particle events, including the NASA reference event, through the application of numerical simulations with the Geant4 Monte-Carlo framework. An evaluation of the shielding effect of lunar regolith was carried out. For the solar particle events a shielding of more than 4 g/cm^2 of regolith would reduce the expected dose to below the current 30-day limits and a shielding of more than 10 g/cm^2 would result in a safety margin factor of two. For GCR adding additional mass shielding did not reduce the absorbed dose significantly. The estimated total dose equivalent received utilizing around 180 g/cm^2 of regolith amounted to 200 mSv/year, which is only about 25% below the corresponding estimates for an unshielded environment. The comparison to model and experimental data from literature showed reasonable agreement to measurements but the analysis of various earlier model results revealed, that substantial differences between the models exist, despite all improvements that have been achieved in recent years.

Plain Language Summary The radiation exposure on the lunar surface is constantly elevated compared to the Earth due to galactic cosmic radiation. Radiation levels can spike on a time scale of hours to days due to solar energetic particle events. To protect astronauts against negative impacts, space agencies have limits against radiation in place. This work investigated the expected background radiation level on the lunar surface and the impact of large solar events and the effectiveness of regolith shielding against this radiation. A comparison against model and experimental data from literature was performed.

Key Points:

- The radiation exposure on the lunar surface from galactic cosmic rays and solar energetic particles was predicted with model calculations
- The effectiveness of regolith shielding against cosmic radiation was investigated
- A comprehensive summary of and comparison against available model and experimental data from literature was performed

Correspondence to:
D. Matthiä,
daniel.matthiae@dlr.de

Citation:
Matthiä, D., & Berger, T. (2024). Radiation exposure and shielding effects on the lunar surface. *Space Weather*, *22*, e2024SW004095. https://doi.org/10.1029/2024SW004095

Received 26 JUL 2024
Accepted 8 NOV 2024

Author Contributions:
Conceptualization: Daniel Matthiä, Thomas Berger
Data curation: Daniel Matthiä
Formal analysis: Daniel Matthiä
Funding acquisition: Thomas Berger
Methodology: Daniel Matthiä, Thomas Berger
Project administration: Thomas Berger
Software: Daniel Matthiä
Validation: Daniel Matthiä
Visualization: Daniel Matthiä, Thomas Berger
Writing – original draft: Daniel Matthiä, Thomas Berger
Writing – review & editing: Daniel Matthiä, Thomas Berger

1. Introduction

Space is a harsh environment and especially the impact of energetic particle radiation on humans is deemed to be one of the major obstacles for future long-term human exploration missions (Durante & Cucinotta, 2011). The radiation environment in space is composed mostly of the omni-present galactic cosmic radiation (GCR), which is modulated in its intensity during the solar activity cycle and which gives rise to a permanent background radiation that is strongest in free space but is also present in low-Earth orbit (LEO) and can even be measured on ground. For long duration exploration missions outside LEO, GCR constitutes the primary source for an increased risk of stochastic radiation effects which implies a greater risk to humans of contracting exposure induced cancer. Another source of dangerous radiation is provided by the protons that are accelerated during a solar particle event (SPE). Astronauts on-board the International Space Station (ISS) are protected against high doses from these SPEs as a result of being shielded by the geomagnetic field along much of the spacecraft trajectory (Berger et al., 2018). This will not be the case for trajectories in free space (Zeitlin et al., 2013) or on the surface of planetary bodies without a magnetic field, such as the Moon and Mars (Ehresmann et al., 2018). For these missions SPEs will be the only potential source of deterministic radiation effects (commonly summarized under the term "radiation sickness") the occurrence of which is linked to specific threshold values.

On Earth, humans are protected from the space radiation field by the atmosphere and, in addition, the Earth's magnetic field provides a highly effective shield against charged particles in low inclination orbits in LEO as, for instance, flown by the ISS. The magnitude of the shielding effect of the magnetosphere depends on the location and reaches its maximum along the geomagnetic equator, where protons, for instance, with energies up to 10 – 15 GeV are deflected by the magnetic field. Even on Mars, its thin atmosphere would provide an effective

10.1029/2024SW004095

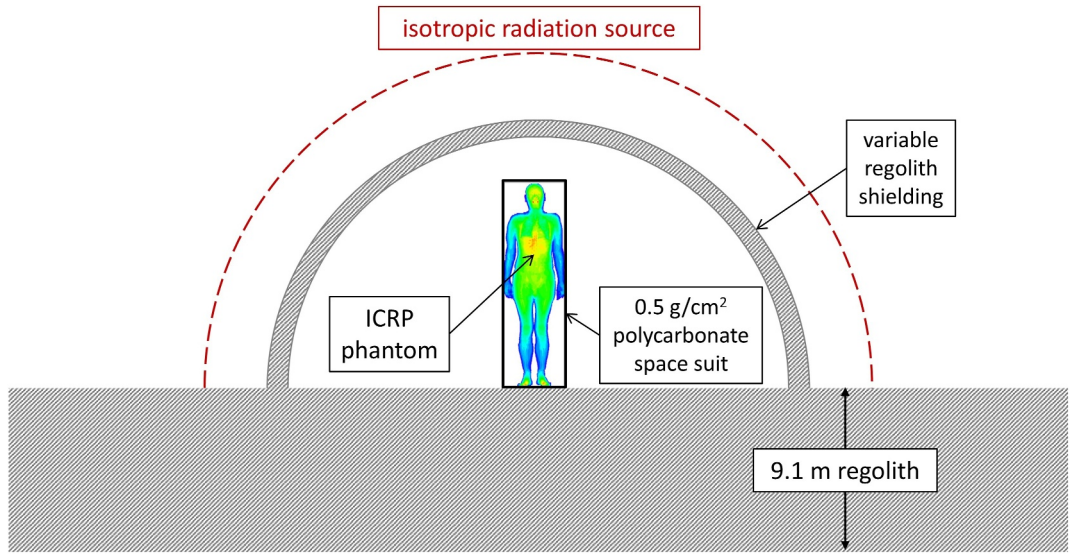

Figure 1. Simulation setup for a male ICRP phantom in a stylized space suit on regolith and protected by variable thickness (0 –20 g/cm^2 for solar particle events; 0–180 g/cm^2 for galactic cosmic radiation) of regolith contained in a half sphere configuration above the phantom. The color code of the phantom indicates the projected density along the ventral-dorsal axis.

protective mechanism especially against SPEs (Ehresmann et al., 2018; Zeitlin et al., 2018). On the surface of the Moon, on the other hand, neither an atmosphere nor a magnetic field exists, thereby leaving humans unprotected but for the shielding they bring or create themselves (Zhang et al., 2020). Aboard a spacecraft in lunar orbit the use of material to create mass shielding is heavily limited by technical constraints. Humans on the lunar surface could in theory use in situ resource material to create a radiation shelter. The building of such a shelter constitutes a significant challenge and naturally the question arises what minimum amount of material would create an acceptable radiation environment for a long-term stay on the lunar surface. In this context, the present work investigates the effectiveness of regolith shielding against the primary GCR background and the contribution of SPEs.

2. Method of Calculating Radiation Exposure Behind Shielding

2.1. Model Calculations Using the ICRP Anthropomorphic Voxel Phantom

In this case, the radiation exposure on the lunar surface was calculated using a similar approach to that described in Reitz et al. (2012). Primary particles were transported through the defined shielding geometry using Geant4 version 11.00. p04 (Agostinelli et al., 2003; Allison et al., 2006, 2016) using the QGSP_INCLXX_HP_EMZ physics list. The shielding geometry consisted of a block of regolith (density 3 g/cm^3, with composition identical to that used in Reitz et al. (2012), i.e. having a length of 20 m and a thickness of 9.1 m. The ICRP male reference phantom (ICRP, 2009) in voxel representation was placed on this block covered by a stylized space suit (polycarbonate, cylindrical shape, thickness 0.5 g/cm^2). A sketch of the simulation setup is provided in Figure 1.

To estimate the effect of a simple habitat or shelter on the radiation exposure, calculations were performed in which half spheres characterized by different thicknesses of regolith were added, each configured to cover the hemisphere above the phantom. Half spheres with inner radii of 2 m were used with radial thicknesses corresponding to 1, 5, 10 and 20 g/cm^2 (i.e., 0.33, 1.66, 3.33, and 6.66 cm of regolith) to calculate the dose from solar energetic particle events. In addition to these, half spheres with thicknesses of 45, 90 and 180 g/cm^2 (i.e., 15, 30, and 60 cm of regolith) were employed for calculating the dose rate from GCR.

After the primary particles were transported through the above described geometries and the production of secondary particles was calculated, the energy deposition and dose in the individual organs was calculated. These organs are represented by a number of assigned voxels in the ICRP reference phantom. The absorbed dose was calculated as the quotient of energy deposition and organ mass ($D = E_{dep}/m$). Finally, using the linear energy transfer of a particle depositing energy, the quality factor (Q) for each energy deposition was calculated and the

dose equivalent derived. The resulting organ dose equivalent was then calculated as the sum of the dose equivalent in all voxels assigned to the organ. The organ dose equivalent can be expressed by the organ absorbed dose times Q, the mean quality factor ($H = Q*D$). Equally, using the relative biological effectiveness (RBE) of the particle depositing energy (as defined in NCRP (2000)), the corresponding gray-equivalent (here denoted as G), relevant for deterministic effects, was calculated by multiplying each energy deposition by the RBE of the particle.

2.2. Model Calculations Using the ICRP Fluence-To-Dose Conversion Coefficients

For the exposure from GCR a second set of calculations was performed in which the voxel phantom was removed and the particle fluence rates inside the regolith shelter and inside the stylized spacesuit through a sphere with radius 30 cm centered at the previous center position of the phantom were recorded. These particle fluence rates were used in combination with the fluence-to-dose conversion coefficients defined by the ICRP (ICRP, 2009, 2013) to calculate the dose and dose equivalent rates. For this purpose, the particle fluence rates of ions ($Z = 1$–26), neutrons, e^-/e^+, photons, μ^-/μ^+, π^-/π^+ were folded with the corresponding conversion coefficients. The advantage of this approach is that the statistical uncertainties are much lower, especially for smaller organs, if the conversion coefficients are understood as defined by the ICRP without statistical uncertainty. Otherwise, in case of the direct calculation of the dose of small organs and heavy shielding the statistical uncertainties can be rather large for a reasonable computational effort due to a relatively low number of hits in the organ. This approach was only applied to the primary GCR irradiation setups, because those contain the transport of heavy ions and cover a much larger energies compared to the SPE calculations, which results in much higher statistical uncertainties.

For this second set of simulations, without the implementation of the ICRP phantom, all primary GCR ions from hydrogen to iron were used and, in contrast to the above described simulation setup, all organs were treated individually in ICRP (2013) which allows for a quantification of the simplifications applied in the first simulation setup.

In addition to the ICRP conversion factors, pre-calculated fluence-to-dose conversion coefficients were used to calculated dose rates in thin slabs (300 μm) of silicon and tissue. Comparing the results of these calculations can be used to estimate the impact of the self-shielding of the body and allows the comparison of experimental data that is often recorded in silicon detectors and converted to tissue or water using a single constant factor.

The results of the calculations with the numerical phantom are presented in Sections 3.1 and 3.2 and compared to the results from the particle fluence to dose conversion in Section 3.2.1. Literature data from experiments and models are discussed in Section 3.3 and compared to the results of this work.

3. Analysis, Results and Discussion

3.1. Solar Particle Events

A number of SPEs were used to estimate the possible radiation exposure incurred by astronauts on the lunar surface as well as the shielding effects provided by utilizing a regolith shelter. The particle spectra were described by double power law functions, the Band-function (Band et al., 1993) as described in Tylka et al. (2010). Of special interest is the SPE that occurred on 4 August 1972 as well as the series of further events that took place between 19 and 24 October 1989. The former had a soft spectrum but extremely high particle intensities at energies below 100 MeV, which means that causes large doses for low mass shielding.

Figure 2 shows the energy spectra of the above mentioned events as described by Tylka et al. (2010), who represented the event on 19 October 1989 by two spectra, one for its earlier phase, that is, the first 23 hr, of the event, labeled in accordance with Tylka et al. (2010) and hereinafter referred to as "19 Oct 89". Similarly, the later phase of the event is labeled hereinafter as "19 Oct 89, ESP," where ESP stands for energetic storm particles. As the different events in the series on 19, 22 and 24 October 1989 occurred within a few days, the cumulative radiation exposure due to these events falls within the 30-day exposure limit set in NASA (2022). Table 1 provides the NASA 30-day permissible exposure limits for short time radiation effects (Table 4.8–1 in NASA (2022)). Other space agencies have identical or similar limits (Shavers et al., 2023). ESA 30-day limits are numerically identical but measured in terms of dose equivalent (Straube et al., 2010).

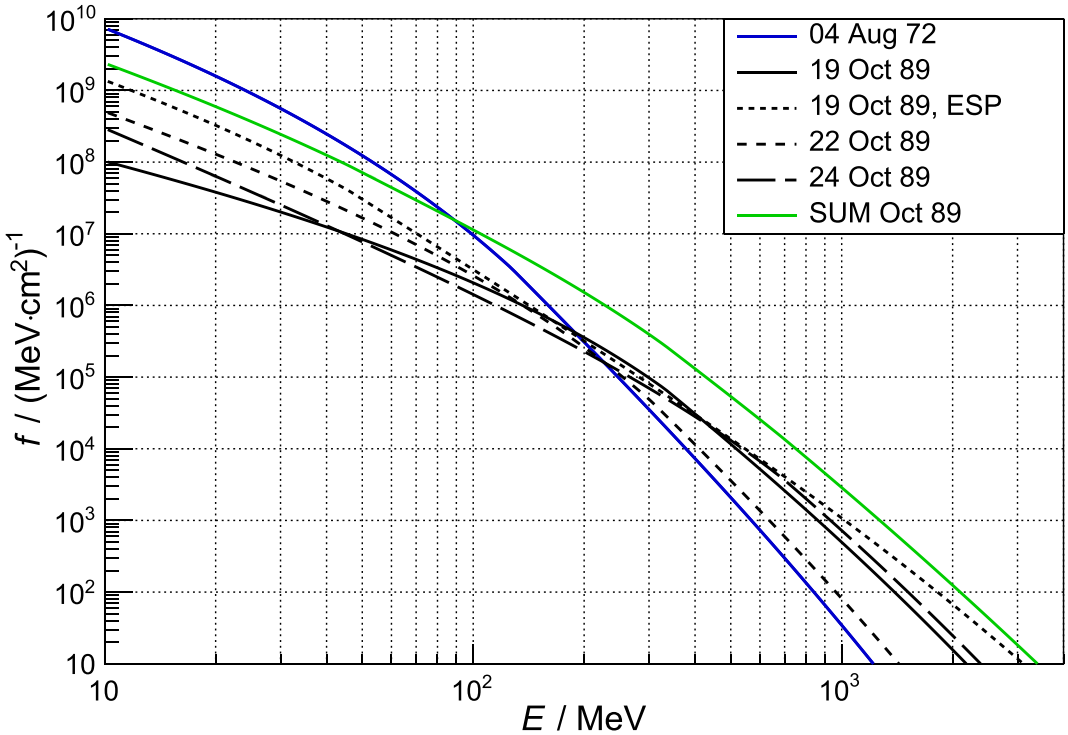

Figure 2. Primary solar energetic proton spectra selected for the study as described in Tylka et al. (2010) and the reference event "SUM Oct 89" (Townsend et al., 2018).

The sum of the proton fluxes for the three events, including the ESP component of the event on 19 October 1989, is represented in Figure 2 by a green line and designated by "SUM Oct 89." The resulting spectrum has a lower intensity at energies below 100 MeV than the event of 4 August 1972 but has a much harder spectrum, which means that more mass shielding would be needed to reduce the radiation exposure from this event compared with the August 1972 event. The sum of the October 1989 events is defined as the design reference SPE environment proton energy spectrum (NASA, 2022; Townsend et al., 2018) relevant for mission planning and shielding design.

Event integrated doses were calculated for all organs inside the ICRP phantom for each of the selected events, including the sum of the October 1989 events. The resulting dose (expressed in mGy-Eq) is shown in Figure 3 for (a) skin and (b) red bone marrow, equivalent to blood forming organs (BFO), compared with the 30-day limits. The lowest shielding indicated in Figure 3 corresponds to that by a person on the lunar surface protected only by a space suit (0.5 g/cm^2). Statistical uncertainties are indicated by error bars in Figure 3 but hardly visible. The relative statistical uncertainties are below 2% for low shielding (spacesuit, 1 g/cm^2) and below 5% for heavier shielding (≥5 g/cm^2).

In a situation of unshielded exposure, the 30-day limits were clearly exceeded for both skin (limit 1.5 Gy-Eq) and red bone marrow (limit 0.25 Gy-Eq) for the August 1972 event and the cumulative October 1989 event. The high intensity at lower energies during the August 1972 event would have led to significantly higher dose to the skin than what would be expected from the cumulative October 1989 event. Due to the self-shielding provided by the body to the inner organs, the dose to red bone marrow from the soft August 1972 event would have been significantly lower than that incurred by the skin, but comparable to the cumulative October 1989 event (~0.5 Gy-Eq). Above a shielding thickness of 4 g/cm^2 (1.3 cm of regolith), all calculated organ dose values fell below the corresponding 30-day limits. However, the dose to red bone marrow due to the cumulative October 1989 event falls right on the limit. To get to a value that lies, for instance, a factor of 2 below the 30-day limit, that is, 0.125 Gy-Eq, the shielding would have to be increased to about 10 g/cm^2 (3.3 cm of regolith).

Table 1
NASA 30-Day Limits for Non-Cancer Risks (NASA, 2022)

Organ	30-Day limit (mGy-Eq)
Lens	1,000
Skin	1,500
Blood Forming Organs (BFO)	250
Circulatory System	250

Note. Data is taken as excerpt from Table 4.8–1 in NASA (2022).

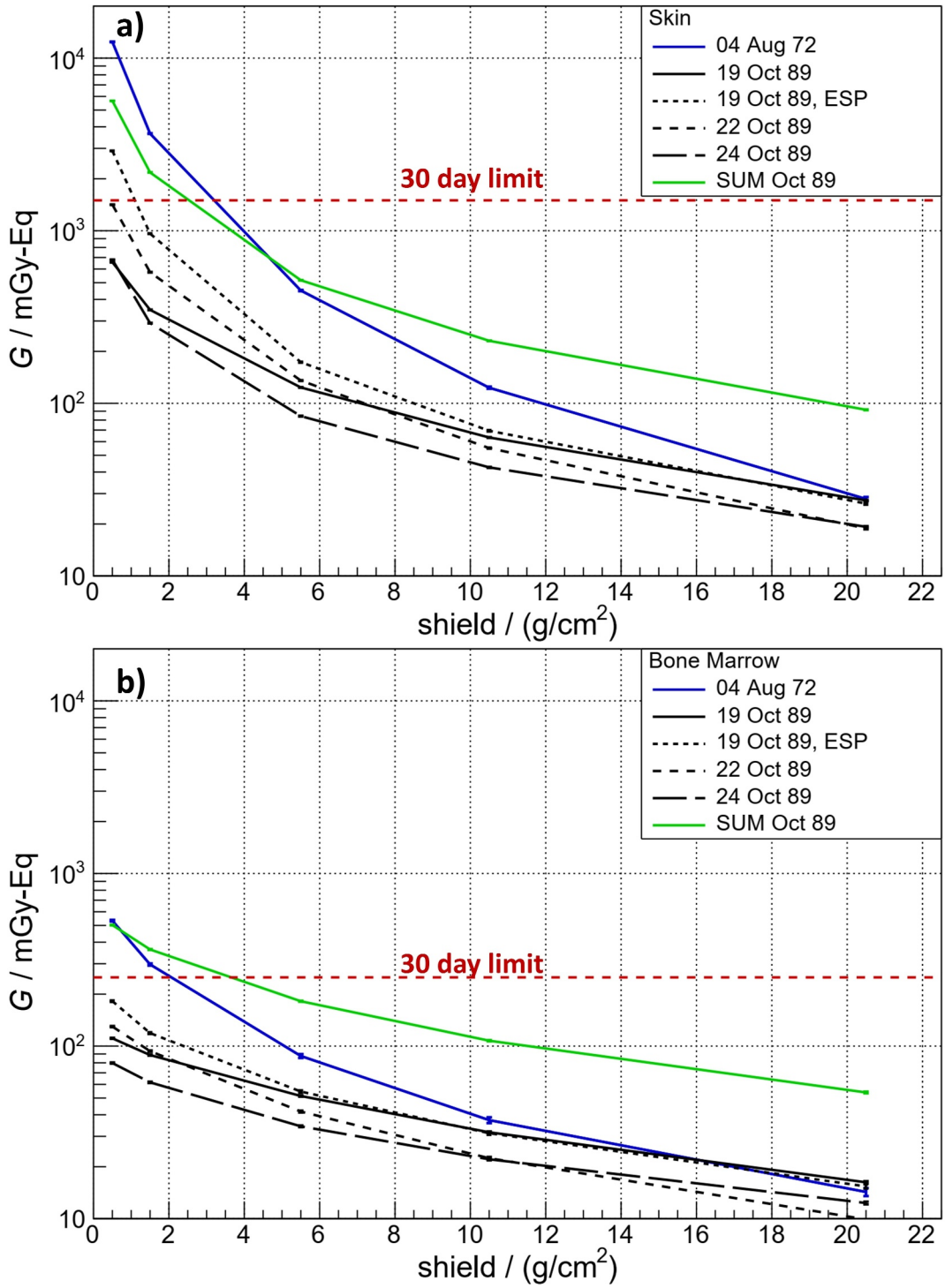

Figure 3. Calculated skin (a) and red bone marrow (b) doses in mGy-Eq versus shielding for the different selected events. The lowest shielding corresponds to the situation of a person on the lunar surface protected only by a space suit (equivalent to 0.5 g/cm^2). Red dashed lines indicate the 30-day limits by NASA (2022) for deterministic effects.

3.2. Galactic Cosmic Radiation

In Reitz et al. (2012) the radiation exposure during solar minimum for a person wearing a space suit at the lunar surface, in otherwise unshielded conditions at solar minimum, was calculated to be about 0.2 mGy/d and

0.6 mSv/d with a corresponding quality factor $Q = 3$. In the present study, this scenario was extended by adding additional shielding mass between 1 and 180 g/cm^2 in the above described geometry.

As the calculations of the full GCR spectrum containing all ions, especially for the heavily shielded scenarios, are computationally extremely extensive, the following simplification was introduced for the case in which the ICRP phantom was placed in the simulation geometry (as described in Section 2.1) and the energy deposition in the phantom was used to calculate the dose rather than the conversion coefficients: The whole-body dose was not calculated from the weighted sum of organ dose applying the tissue weighting factors w_T, which is the definition of the effective dose equivalent (ICRP, 2016), as some human organs have very small volumes and correspondingly small masses. As a consequence, statistical fluctuations in the energy deposition in these organs could lead to large variations and uncertainties in the organ weighted effective dose equivalent. Instead, the absorbed dose rate and dose equivalent rate averaged over the whole ICRP phantom were calculated. As GCR is highly penetrating the radiation exposure throughout the body is expected to be relatively uniform. The calculated organ dose equivalent rates in Reitz et al. (2012) showed mostly variations of ±20% around the calculated effective dose equivalent rate. As the radiation exposure within the body is expected to be lower for the inner organs and those organs have the greatest weighting factors within the effective dose equivalent, the body averaged dose equivalent can be expected to provide a conservative estimation for the effective dose equivalent for GCR irradiation. As a cross-check for the accuracy of approximating the effective dose equivalent by the whole-body dose equivalent, the calculation of the effective dose equivalent using the ICRP conversion coefficients with the particle fluences, as described in Section 2.2, was included in this work.

The primary GCR spectra were calculated for solar minimum conditions, that is, GCR maximum intensity, using the model from Matthiä et al. (2013) and ions with $Z = 1$–26 were considered in the energy range from 10 MeV/nucleon to 200 GeV/nucleon.

In Figure 4 the resulting absorbed dose rates and dose equivalent rates are presented together with the corresponding quality factor. The absorbed dose rate increases from 0.25 mGy/d (~90 mGy/year) for the spacesuit shielding to about 0.28 mGy/d (~100 mGy/year) for shielding between 40 and 90 g/cm^2. At higher shielding levels the dose rate slowly decreases but hardly reaches values below the initial 0.25 mGy/d, even for that scenario calculated with the highest shielding (180 g/cm^2). The estimated dose equivalent rate in the unshielded scenario is 0.84 mSv/d (~310 mSv/year), which is about 25% greater than the estimate of the effective dose equivalent in Reitz et al. (2012). The dose equivalent rate drops and reaches a local minimum of 0.6 mSv/d (~220 mSv/year) at around 20 g/cm^2.

The decrease in the dose equivalent rate is due to the fragmentation of primary GCR ions that have a high quality factor and goes along with a steep decrease in the average quality factor of the radiation field (Figure 4b). This effect was also predicted to occur in other scenarios of GCR exposure, like LEO as given in Matthiä et al. (2013) and in interplanetary space as calculated by (Slaba et al., 2013, 2017). Above a minimum in the quality factor, that is reached at 45 g/cm^2, a steady and slight increase in Q is predicted which can be attributed to the formation of a secondary neutron field. At higher shielding (90 g/cm^2) the dose equivalent rate increases up to 0.65 mSv/d (~240 mSv/year).

It should be noted that this maximum is not very well defined in the calculations presented here, as the shielding values that were included in the simulation were relatively widely spaced at 45, 90 and 180 g/cm^2. From the trend it is quite plausible, that the dose equivalent could increase some more above 90 g/cm^2. For the highest shielding the absorbed dose equivalent dropped to 0.55 mSv/d (~200 mSv/year) and can be expected to drop further for increasingly higher amounts of shielding.

3.2.1. Contribution of Different Particle Types to the Galactic Cosmic Radiation Component and Comparison to Fluence-To-Dose Conversion Coefficients

Contributions of different particle types were calculated using the results of folding the particle fluence rate with the fluence-to-dose conversion coefficients. Figure 5 contains the total absorbed dose rates (a) and total effective dose equivalent rates (b) calculated with the ICRP phantom implemented in the simulation (ICRP, phantom total) and derived from the particle fluence rates (ICRP conversion coeff., total) together with the contribution of the different components of the radiation field. The heavy ion component contains nuclei heavier than helium and

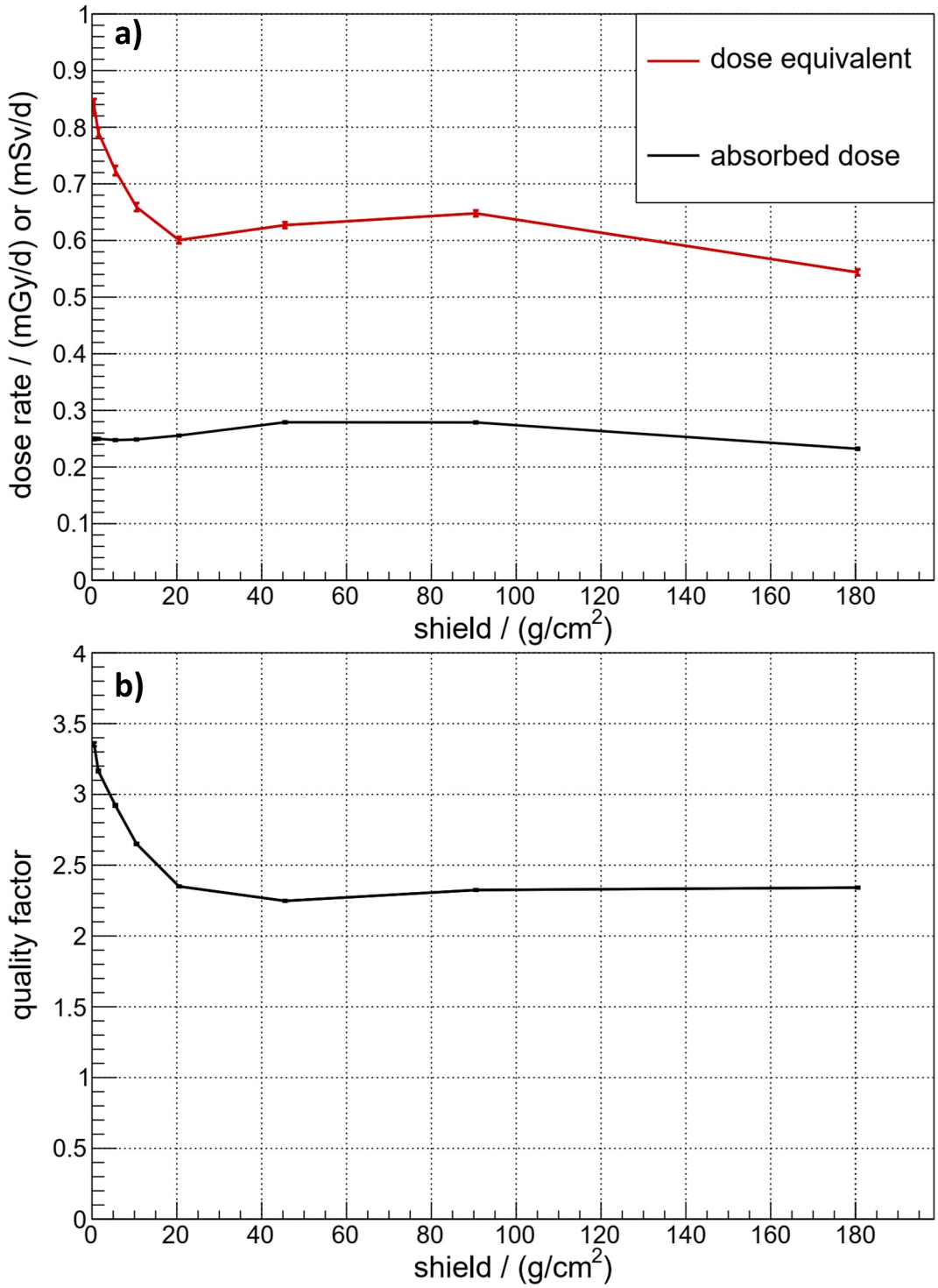

Figure 4. Calculated absorbed dose rates and dose equivalent rates (a) and the corresponding quality factor (b) calculated for solar minimum galactic cosmic radiation conditions over the whole body of the ICRP phantom.

deuteron, triton and ^{3}He, as well. The figure illustrates how the radiation field changes with increasing regolith shielding.

Protons are clearly the most important component to the absorbed dose, especially at regolith shielding up to 20 g/cm^2; in this range about 60% of the dose originates from protons. The proton fraction decreases at higher

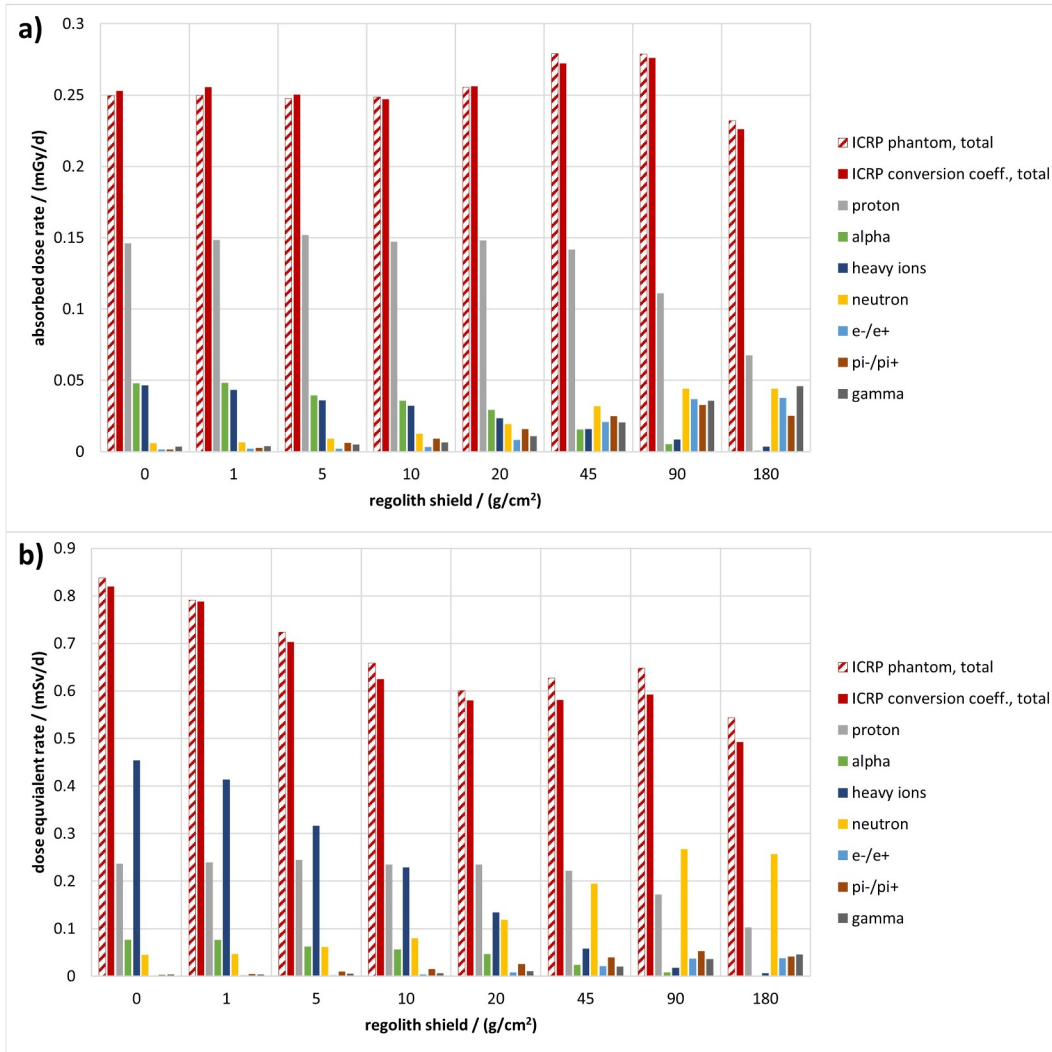

Figure 5. Contribution of different particle types to the absorbed dose rate (a) and the effective dose equivalent rate (b). Particle contributions were calculated from particle fluence inside the regolith shielding using ICRP conversion coefficients. The total dose calculated from conversion coefficients and using the implementation of the ICRP phantom in the simulation is also shown for comparison. Dose equivalent rate refers to whole body dose equivalent in case of the ICRP phantom implementation and to effective dose equivalent in case of conversion coefficients.

shielding but remains the single most important contributor. Other important components to the absorbed dose at low shielding are alpha particles and heavy ions, which both contribute between 15% and 20%. At a shielding of 45 g/cm^2 and above, the most important components next to protons are neutrons, electrons/protons (e^-/e^+), pions (pi^-,pi^+) and gammas, each contributing between 10% and 20%. For the dose equivalent, the most important contribution at shielding below 10 g/cm^2 is heavy ions and protons. At these shielding values protons, alphas and heavy ions contribute 90% or more to the total dose equivalent. At higher shielding the importance of neutrons increases reaching approximately 50% at 180 g/cm^2.

For the total dose, the results of the calculation with the ICRP phantom and the conversion coefficients agree within 10% at 180 g/cm^2 and about 2% for the space suit calculation. This supports the assumption, that calculating the whole body absorbed dose and dose equivalent for the ICRP phantom provides a reasonable estimate for the effective dose equivalent.

3.3. Comparison With Model and Experimental Data From Literature

In this section the results of this work are discussed in the context of available literature data, including both earlier model predictions and available measurement data. A number of publications exist on the topic covering different aspects of the problem of the potential radiation exposure on the lunar surface. A comparison of available literature data is complicated by the different approaches of the authors, in case of the model calculations these include among others.

- differences in the primary particle models or the selected solar events,
- differences in shielding geometries and materials,
- differences in dose quantities, for example, organ dose equivalent versus gray-equivalent, effective dose versus effective dose equivalent or different definitions of the quality factor.

Here, we try to select data from publications that are, in terms of model setup and target quantities, comparable to the results of this work and put them in context. Most articles contain a large amount of additional information and the interested read is referred to the original publications for the details. Selected results of a number of model calculations available in literature are summarized in Table 2 and discussed in the following.

An early study of the expected radiation exposure of solar energetic particle events on the radiation exposure on the lunar surface and the effectiveness of regolith shielding was (NASA, 1988), in which the exposure from three different SEP events were estimated, including the August 1972 event. The dose equivalent rates for different shielding geometries (spherical, cylindrical, planar) were calculated in NASA (1988) in 5 cm depth in tissue, representative for BFO, and using a now outdated definition of the quality factor from ICRP (1977). The values from NASA (1988) exceed the result of this work by far. For no shielding by a factor of about 8, for heavier shielding by more than 20. Explanations for theses discrepancies could be among others: advancement in transport models, differences in the energy range of the primary particles or that the 5 cm depth in tissue are not representative of BFO. A later study (Slaba et al., 2011) investigated specifically the neutron dose during this event and estimated an effective dose from neutrons of 25.1 mSv for this event, which is about a factor of five greater than the value calculated in this work.

A recent work (Shavers et al., 2023) investigated the predictions of the standard tools of different space agencies for the dose rates for a lunar mission. They found that the estimates for the effective dose from GCR agree within approximately 30% and the sum of the GCR exposure and the reference SPE within about a factor of 2. The results of this work lie within the ranges of the dose rates given in Shavers et al. (2023). Converted to yearly doses, the range of effective dose equivalent rates in Shavers et al. (2023) extends from 192 mSv/year to 232 mSv/year for solar minimum behind 5 g/cm^2 Al shielding. The result of Burahmah and Heilbronn (2023) of 278 mSv/year (762.1 μSv/d) are compatible with these values, considering the fact, that they calculated for greater GCR intensity and slightly lower shielding.

Hayatsu et al. (2008) calculated the ambient dose equivalent H*(10), which is an operational quantity for terrestrial radiation protection and meant to estimate the effective dose (ICRP, 1991; ICRU, 1993). Their result agrees well with the effective dose equivalent rate calculated in this work for GCR solar minimum but a substantially greater neutron dose was calculated, approximately a factor 4 to 5. Naito et al. (2020) calculated a neutron dose rate, that is a factor 2 lower compared to Hayatsu et al. (2008) but a total effective dose equivalent that is about 40% greater than the value from Hayatsu et al. (2008), Burahmah and Heilbronn (2023) and this work.

Effective dose equivalent rates in the lunar surface behind aluminum shielding and subsurface were also most recently estimated by Dobynde and Guo (2024) using calculations on a spherical phantom. Their values are about 40%–50% greater than the results of this work, Burahmah and Heilbronn (2023) and Hayatsu et al. (2008) for corresponding amounts of regolith shielding, but compatible with Naito et al. (2020).

In total, it can be concluded, that while many model results show good agreement with the results of this work, substantial discrepancies remain in some parts. Especially the application of different model geometries and shielding and various dose quantities used by the authors make a systematic comparison complicated. Discrepancies in the neutron dose calculated in this work with data from literature, for instance, could be possibly explained by the irradiation geometry used in the model calculations. The limited extent of the simulation geometry could lead to an underestimation of neutrons produced or backscattered in locations further away.

Table 2
Modeled Dose Rate Data From Literature Compared to Values From This Work

Literature data					This work		
Ref. #	Source	Shielding(s)	Quantity/unit	Value(s)	Quantity/unit	Value	Notes
NASA (1988), estimated from Figure 5	1972 SEP	0, 5, 10 and 20 g/cm^2 regolith	BFO dose equivalent, mSv	$4.0{\cdot}10^3$, $1.9{\cdot}10^3$, $8.6{\cdot}10^2$, $2.3{\cdot}10^2$	BFO dose, mGy-Eq, 0; 5; 10 and 20 g/cm^2 regolith	533 ± 6; 88 ± 2; 37 ± 1; 14.3 ± 0.8	NASA (1988) data was converted from rem to mSv. Data for low shielding (<10 cm regolith) in NASA (1988) is only available in graphical form for planar shielding with normal incidence of primaries and was read from Figure 5 of the publication. Results of this work include the space suit shielding in addition to the regolith shielding.
Slaba et al. (2011), Table 3, average	1972 SEP	none	Neutron effective dose/mSv	25.1	Neutron effective dose equivalent/mSv	5.6 ± 0.30.1	The values from Slaba et al. (2011) are averages for 12 different regolith compositions, all differing by less than 5% from the average. Dose rates from this work were calculated with the ICRP fluence-to-dose conversion coefficients using the quality fractor definde by ICRP. No data from this work for solar maximum conditions
	GCR solar min.	none	Neutron effective dose rate/(mSv/year)	48.3	Neutron effective dose equivalent rate/(mSv/year)	16.2 ± 0.3	
	GCR solar max.	none	Neutron effective doserate/(mSv/year)	21.9	–	–	
Burahmah and Heilbronn (2023), Table 2, Lunar surface, male	GCR solar min.	1 cm (2.33 g/cm^2) Al	Total effective dose rate/(μSv/d)	762.1	Total effective dose equivalent rate/(μSv/d)	768 ± 8	Values for this work have been obtained by interpolating the results at 1 and 5 g/cm^2 regolith shielding. No data from this work for solar maximum
	GCR solar max.	1 cm (2.33 g/cm^2) Al	Total effective dose rate/(μSv/d)	260.8	–	–	
Shavers et al. (2023), Table 5 for GCR, Table 6 for GCR + Reference SPE, JAXA male, NASA male, RSA	GCR, Jan. 2013	5 g/cm^2 Al	30-day total effective dose/mSv (JAXA/NASA/RSA)	19.1/14.8/15.8	30-day total effective dose equivalent/mSv	15.8 ± 0.1	Model calculations were rerun as described above but with boundary conditions from Shavers et al. (2023), that is, January 2013 for GCR and Oct. 1989 reference SPE and Al shielding.
	GCR, Jan. 2013	20 g/cm^2 Al	30-day total effective dose/mSv (JAXA/NASA/RSA)	16.8/13.5/13.8	30-day total effective dose equivalent/mSv	13.9 ± 0.1	
	GCR, Jan. 2013 + Reference SPE	5 g/cm^2 Al	30-day total effective dose/mSv (JAXA/NASA/RSA)	173/207/328	Reference SPE effective dose/mSv	238 ± 1	Model calculations were rerun as described above but with boundary conditions from Shavers et al. (2023), that is, January 2013 for GCR and Oct. 1989 reference SPE and Al shielding
	GCR, Jan. 2013 + Reference SPE	20 g/cm^2 Al	30-day total effective dose/mSv (JAXA/NASA/RSA)	60.5/85.4/94.6	Reference SPE effective dose/mSv	69.8 ± 0.6	Values are the sum of GCR contribution and the NASA reference SPE.

Table 2
Continued

Literature data					This work		
Ref. #	Source	Shielding(s)	Quantity/unit	Value(s)	Quantity/unit	Value	Notes
Hayatsu et al. (2008), Table 2	GCR, solar min.	none	H*(10)/(mSv/yr)	310 (total) 72.9 (neutron) 3.3 (gamma)	Effective dose equivalent rate/(mSv/yr)	299 ± 6 (total) 16.2 ± 0.3 (neutron) 1.35 ± 0.01 (gamma)	Values for this work are for space suit only shielding without regolith and calculated with the ICRP conversion coefficients
Naito et al. (2020), Table 2	GCR, solar min.	none	Effective dose equivalent rate/(mSv/yr)	416 ± 18 (total) 40 ± 4 (neutron)	Effective dose equivalent rate/(mSv/yr)	299 ± 6 (total) 16.2 ± 0.3 (neutron)	
Dobynde and Guo (2024), Figure 1	GCR, solar min.	1 g/cm^2 Al; 10 g/cm^2 Al; 30 g/cm^2 Al; 60 g/cm^2 Al;	Dose equivalent rate in spherical phantom (mSv/yr)	411; 349; 311; 322;	Effective dose equivalent rate/(mSv/yr); 1 g/cm^2 regolith; 10 g/cm^2 regolith; 30 g/cm^2 regolith; 60 g/cm^2 regolith;	288 ± 6; 228 ± 4; 212 ± 3; 213 ± 2;	Values from Dobynde and Guo (2024) for the lunar surface for different values of extra Al shielding were used and converted to mSv/yr. Data from this work were calculated with ICRP conversion coefficients and interpolated between the different regolith shielding values, where necessary to match the shielding values from Dobynde and Guo (2024)

A direct comparison to experimental data is difficult, due to the sparsity of available measurements and the fact that measurements are made under different conditions compared to the modeled boundary conditions. Also, no data from the lunar surface or orbit is available for the historic particle events, that were discussed above. The dose rate measurements available from lunar surface (Zhang et al., 2020) and lunar orbit (Dachev et al., 2011; Spence et al., 2010) have been performed with silicon detectors which are expected to differ from the above presented calculated doses through three major factors.

- Silicon detectors have a low sensitivity to neutrons,
- the dose in silicon of charged particles differs from the dose in water or tissue in the same radiation field and needs to be converted and
- the phantom used in the model calculations provides additional shielding that modifies the radiation field compared to the measurement in a thin silicon detector.

In order to obtain comparable values from the model calculations, the particle fluence rates calculated in the unshielded scenario described above outside of the polycarbonate space suit were used in combination with pre-calculated conversion coefficients for all particle types. The conversion coefficients were calculated with Geant4 for an isotropic irradiation of 0.3 mm thick slabs of silicon and tissue and for all particle types under consideration.

Available data measured in moon orbit with silicon detectors is available from the RADOM experiment on Chandrayaan-1 (Dachev et al., 2011) for 2009 and from CRaTER on the Lunar Reconnaissance Orbiter Mission (Spence et al., 2010). Values measured in orbit can be used to approximate the dose on the surface by considering a geometrical shielding factor calculated from the altitude of the spacecraft above the surface or scaling the values from the surface by the inverse. Values of measurements during solar minimum conditions in 2009 are given in Table 3. The model values from this work calculated for a 0.3 mm silicon slab agree reasonably well with the measurement by the CRaTER instrument, which were scaled to the lunar surface, but overestimate the measurement of RADOM in lunar orbit by about 30%. The two measurements, however, are for unknown reasons inconsistent between each other, as well.

Table 3
Measured Dose Rate Data From Literature Compared to Values From This Work

Literature data				This work		
Ref. #	Source	Quantity/unit	Value(s)	Quantity/unit	Value	Notes
Dachev et al. (2011)	GCR, solar min. (Mai 2009–Oct 2009)	Dose rate in Si μGy/h	10.7	Dose rate in Si μGy/h	13.4 ± 0.1	Dose rate from the final 3 months of the mission (2009-05-20 to 2009-08-28) at 200 km altitude orbit. The result of this work was obtained from the simulation without regolith shielding and an additional factor of 0.72/0.5 to account for the reduced geometrical shielding by the moon at 200 km altitude (0.72) compared to the surface (0.5). The measurement of Dachev et al. (2011) is expected to underestimate the true value due to the limited sensitivity range in the measured energy deposition.
Spence et al. (2010); https://crater-web.sr.unh.edu	GCR, solar min. (December 2009)	Dose rate in Si μGy/h	9.86 ± 0.02	Dose rate in Si μGy/h	9.3 ± 0.1	CRaTER data (D1&D2 dose rate from https://crater-web.sr.unh.edu) was averaged over Dec 2009. A factor of 1/1.33 (as provided in the data) was used to calculate back to the dose rate in the Silicon detector. The result of this work was obtained from the simulation without additional regolith shielding. CRaTER data is provided by default as an estimate for the dose on the lunar surface using an altitude dependent correction factor.
Zhang et al. (2020)	GCR, low solar modulation (Jan/Feb 2019)	Dose rate in Si μGy/h	10.2 ± 0.9 (charged) 3.1 ± 0.5 (neutral)	Dose rate in Si μGy/h	9.2 ± 0.1 (charged) 0.0730 ± 0.0003 (neutral)	Modeled dose rate from this work for neutral particles is the sum neutrons and photons
	GCR, low solar modulation (Jan/Feb 2019)	Dose equivalent rate in water μSv/h	57.1 ± 10.6 (charged)	Dose equivalent rate in tissue μSv/h	64.7 ± 0.8 (charged) 3.33 ± 0.02 (neutral)	Zhang et al. (2020) used a factor of 1.3 to convert the measured dose of charged particles in Si to dose in water and a quality factor of $Q = 4.3 \pm 0.7$. Dose equivalent rate from this work was calculated from isotropic irradiation of a slab of tissue using particle spectra from the simulation without additional regolith shielding. The conversion factor from dose in Si to dose in water for charged particles calculated from the model is 1.21.

Dose rates were measured by the Lunar Lander Neutrons and Dosimetry (LND) experiment during the Chang'E 4 mission (Zhang et al., 2020). The dose rates measured in January 2019 agree with the results of this work within the error bars. LND also provides the only experimental estimate of a dose equivalent rate from charged GCR particles on the lunar surface: 57.1 ± 10.6 μSv/h. From the model of this work a corresponding value of 64.7 ± 0.8 μSv/h was calculated. If the contribution of neutral particles is neglected (~5%), this value is about a factor of 1.9 greater than the calculated whole-body dose equivalent of 0.84 mSv/d (35 μSv/h), which means that the self shielding of the body reduces the effective dose equivalent by almost 50% compared to a measurement taken with a thin detector.

4. Summary

In this work, the radiation exposure that can be expected on the lunar surface for a worst-case scenario, that is: under solar minimum conditions with contributions from a number of historical solar particle events, was estimated using numerical simulations performed with Geant4.

The effectiveness of a semi-spherical regolith shielding between 0 and 20 g/cm^2 for SPEs and between 0 and 180 g/cm^2 for GCR, in combination with a space suit (0.5 g/cm^2) was investigated.

It was found that shielding above a few centimeters of regolith would effectively reduce the radiation exposure to skin and red bone marrow (BFO) to levels well below the current 30-day limits for deterministic effects. On the other hand, for a lightly shielded environment and especially in the scenario in which an astronaut would be

protected only by a space suit, the estimated dose values could reach a multiple of the limit or, in case of the skin dose, could be even more than an order of magnitude greater. This suggests that in such a case the radiation exposure could reach critical levels even if an astronaut were exposed to only a fraction of the event, for instance before reaching shelter.

In contrast to solar particle events, for which mass shielding is very effective, the absorbed dose rate from GCR is not expected to decrease significantly with additional shielding. For a solar minimum scenario, the calculated whole body absorbed dose rate is relatively constant over the investigated thickness, that is, between 0 and 180 g/cm^2 at a level of 0.25 to 0.28 mGy/d (approximately 90 to 100 mGy/year).

The whole-body dose equivalent rate as an estimate of the effective dose equivalent rate is effectively reduced by the first 10 g/cm^2 of regolith through the fragmentation of primary heavy ions and the related reduction of the quality factor from about 3.4 to 2.3. For higher shielding the dose equivalent rate increases due to secondary particle production while the quality factor increases only slightly due to the formation of the secondary neutron field. An additional shielding effect is only visible at values above 90 g/cm^2. Nevertheless, the calculated dose rate even at 180 g/cm^2 (0.55 mSv/d or 200 mSv/year) is only 35% below the value for the unshielded scenario (0.84 mSv/d or 310 mSv/year). Calculations using the pre-defined fluence-to-dose conversion showed a good agreement within 10% with the calculations using the implementation of the ICRP reference voxel phantom in the simulations.

The comparison of the model results with model data from literature is ambiguous. While large differences between the results and published data from decades ago (NASA, 1988) exists, more recent data show better agreement, specifically data from this work and the interagency comparison by Shavers et al. (2023), which shows the progress in model capabilities. However, there are still discrepancies between recent publications of up to 50% in the total effective dose equivalent or comparable quantities from the exposure of GCR, even under low shielding conditions where agreement should be best. Specifically, the neutron contribution to the effective dose equivalent differs between different models.

Comparisons of the model results of this work with experimental data show mostly good agreement but is limited to the available data measured with silicon detectors. The analysis of the dose equivalent estimated by LND and the model calculation for a tissue slab compared to the anthropomorphic phantom suggests that the self-shielding effect on the lunar surface for GCR leads to an about 50% lower effective dose equivalent rate compared to the dose in a thin slab. Considering the remaining discrepancies between different models, the necessity for more experimental data persists, especially when it comes to measuring the dose in tissue and the radiation quality factor of the field on the lunar surface.

Data Availability Statement

Data used in the analysis is available at Matthiä and Berger (2024). The Geant4 toolkit for the simulation of the passage of particles through matter that was used in the analysis is available at https://geant4.web.cern.ch/.

Acknowledgments
The work was supported by DLR Grant FuE-Projekt ''ISS LIFE'' (Programm RF-FuW, Teilprogramm 475). Open Access funding enabled and organized by Projekt DEAL.

References

Agostinelli, S., Allison, J., Amako, K., Apostolakis, J., Araujo, H., Arce, P., et al. (2003). GEANT4-a simulation toolkit. *Nuclear Instruments and Methods in Physics Research Section A: Accelerators, Spectrometers, Detectors and Associated Equipment*, *506*(3), 250–303. https://doi.org/10.1016/S0168-9002(03)01368-8

Allison, J., Amako, K., Apostolakis, J., Araujo, H., Dubois, P. A., Asai, M., et al. (2006). Geant4 developments and applications. *IEEE Transactions on Nuclear Science*, *53*(1), 270–278. https://doi.org/10.1109/TNS.2006.869826

Allison, J., Amako, K., Apostolakis, J., Arce, P., Asai, M., Aso, T., et al. (2016). Recent developments in GEANT4. *Nuclear Instruments and Methods in Physics Research Section A: Accelerators, Spectrometers, Detectors and Associated Equipment*, *835*, 186–225. https://doi.org/10.1016/j.nima.2016.06.125

Band, D., Matteson, J., Ford, L., Schaefer, B., Palmer, D., Teegarden, B., et al. (1993). BATSE observations of gamma-ray burst spectra. I-Spectral diversity. *The Astrophysical Journal*, *413*, 281–292. https://doi.org/10.1086/172995

Berger, T., Matthiä, D., Burmeister, S., Lee, K., Rios, R. R., Semones, E., et al. (2018). The solar particle event from september 2017 as observed onboard the international space station (ISS). *Space Weather*, *16*(9), 1173–1189. https://doi.org/10.1029/2018SW001920

Burahmah, N. T., & Heilbronn, L. H. (2023). Comparison of doses in lunar habitats located at the surface and in crater. *Aerospace*, *10*(11), 970. https://doi.org/10.3390/aerospace10110970

Dachev, T. P., Tomov, B. T., Matviichuk, Y. N., Dimitrov, P. S., Vadawale, S. V., Goswami, J. N., et al. (2011). An overview of RADOM results for Earth and Moon radiation environment on Chandrayaan-1 satellite. *Advances in Space Research*, *48*(5), 779–791. https://doi.org/10.1016/j.asr.2011.05.009

Dobynde, M., & Guo, J. (2024). Guidelines for radiation-safe human activities on the Moon. *Nature Astronomy*, *8*(8), 991–999. https://doi.org/10.1038/s41550-024-02287-8

Durante, M., & Cucinotta, F. A. (2011). Physical basis of radiation protection in space travel. *Reviews of Modern Physics*, *83*(4), 1245–1281. https://doi.org/10.1103/RevModPhys.83.1245

Ehresmann, B., Hassler, D. M., Zeitlin, C. J., Guo, J., Wimmer-Schweingruber, R. F., Matthiä, D., et al. (2018). Energetic particle radiation environment observed by RAD on the surface of Mars during the September 2017 event. *Geophysical Research Letters*, *45*(11), 5305–5311. https://doi.org/10.1029/2018GL077801

Hayatsu, K., Hareyama, M., Kobayashi, S., Yamashita, N., Miyajim, M., Sakurai, K., & Hasebe, N. (2008). Radiation doses for human exposed to galactic cosmic rays and their secondary products on the lunar surface. *Biological Sciences in Space*, *22*(2), 59–66. https://doi.org/10.2187/bss.22.59

ICRP. (1977). Recommendations of the ICRP. *Annals of the ICRP*, *1*(3), 1–53.

ICRP. (1991). 1990 recommendations of the international commission on radiological protection. *Annals of the ICRP*, *21*(1–3), 1–201.

ICRP. (2009). ICRP publication 110: Adult reference computational phantoms. *Annals of the ICRP*, *39*(2).

ICRP. (2013). ICRP, 123. Assessment of radiation exposure of astronauts in space. ICRP Publication 123. *Annals of the ICRP*, *42*(4), 1–339. https://doi.org/10.1016/j.icrp.2013.05.004

ICRP. (2016). ICRP Publication 132: Radiological protection from cosmic radiation in aviation. *Annals of the ICRP*, *45*(1), 5–48. https://doi.org/10.1177/0146645316645449

ICRU. (1993). ICRU report 51: Quantities and units in radiation protection dosimetry. *Journal of the ICRU*, *26*(2).

Matthiä, D., & Berger, T. (2024). *Radiation exposure and shielding effects on the lunar surface*. Authorea Preprints. https://doi.org/10.5281/zenodo.13365755

Matthiä, D., Berger, T., Mrigakshi, A. I., & Reitz, G. (2013). A ready-to-use galactic cosmic ray model. *Advances in Space Research*, *51*(3), 329–338. https://doi.org/10.1016/j.asr.2012.09.022

Naito, M., Hasebe, N., Shikishima, M., Amano, Y., Haruyama, J., Matias-Lopes, J. A., et al. (2020). Radiation dose and its protection in the moon from galactic cosmic rays and solar energetic particles: At the lunar surface and in a lava tube. *Journal of Radiological Protection*, *40*(4), 947–961. https://doi.org/10.1088/1361-6498/abb120

NASA. (1988). Solar-flare shielding with regolith at a lunar-base site (NASA-TP-2869). Retrieved from https://ntrs.nasa.gov/archive/nasa/casi.ntrs.nasa.gov/19910008686.pdf

NASA. (2022). NASA space flight human-system standard volume 1: Crew health. Retrieved from https://standards.nasa.gov/sites/default/files/standards/NASA/B//2022-01-05-NASA-STD-3001-Vol1-Rev-B-Final-Draft-Signature-010522.pdf

NCRP. (2000). NCRP report 132: Radiation protection guidance for activities in low-earth orbit.

Reitz, G., Berger, T., & Matthiae, D. (2012). Radiation exposure in the moon environment. *Planetary and Space Science*, *74*(1), 78–83. https://doi.org/10.1016/j.pss.2012.07.014

Shavers, M. R., Semones, E. J., Shurshakov, V., Dobynde, M., Sato, T., Komiyama, T., et al. (2023). Comparison of dose and risk estimates between ISS partner agencies for a 30-day lunar mission. *Zeitschrift für Medizinische Physik*, *34*(1), 31–43. https://doi.org/10.1016/j.zemedi.2023.10.005

Slaba, T. C., Bahadori, A. A., Reddell, B. D., Singleterry, R. C., Clowdsley, M. S., & Blattnig, S. R. (2017). Optimal shielding thickness for galactic cosmic ray environments. *Life Sciences and Space Research*, *12*, 1–15. https://doi.org/10.1016/j.lssr.2016.12.003

Slaba, T. C., Blattnig, S. R., & Clowdsley, M. S. (2011). Variation in lunar neutron dose estimates. *Radiation Research*, *176*(6), 827–841. https://doi.org/10.1667/rr2616.1

Slaba, T. C., Mertens, C. J., & Blattnig, S. R. (2013). Radiation shielding optimization on Mars. NASA/TP–2013-217983. https://ntrs.nasa.gov/citations/20130012456

Spence, H. E., Case, A. W., Golightly, M. J., Heine, T., Larsen, B. A., Blake, J. B., et al. (2010). CRaTER: The cosmic ray telescope for the effects of radiation experiment on the lunar reconnaissance orbiter mission. *Space Science Reviews*, *150*(1), 243–284. https://doi.org/10.1007/s11214-009-9584-8

Straube, U., Berger, T., Reitz, G., Facius, R., Fuglesang, C., Reiter, T., et al. (2010). Operational radiation protection for astronauts and cosmonauts and correlated activities of ESA Medical Operations. *Acta Astronautica*, *66*(7), 963–973. https://doi.org/10.1016/j.actaastro.2009.10.004

Townsend, L. W., Adams, J. H., Blattnig, S. R., Clowdsley, M. S., Fry, D. J., Jun, I., et al. (2018). Solar particle event storm shelter requirements for missions beyond low Earth orbit. *Life Sciences and Space Research*, *17*, 32–39. https://doi.org/10.1016/j.lssr.2018.02.002

Tylka, A. J., Dietrich, W. F., & Atwell, W. (2010). Assessing the space-radiation hazard in ground-level enhanced (GLE) solar particle events. In *Paper presented at the 2010 fall AGU meeting*.

Zeitlin, C., Hassler, D. M., Cucinotta, F. a., Ehresmann, B., Wimmer-Schweingruber, R. F., Brinza, D. E., et al. (2013). Measurements of energetic particle radiation in transit to Mars on the Mars science laboratory. *Science*, *340*(6136), 1080–1084. https://doi.org/10.1126/science.1235989

Zeitlin, C., Hassler, D. M., Guo, J., Ehresmann, B., Wimmer-Schweingruber, R. F., Rafkin, S., et al. (2018). Analysis of the radiation hazard observed by RAD on the surface of Mars during the September 2017 solar particle event. *Geophysical Research Letters*, *45*(12), 5845–5851. https://doi.org/10.1029/2018GL077760

Zhang, S., Wimmer-Schweingruber, R. F., Yu, J., Wang, C., Fu, Q., Zou, Y., et al. (2020). First measurements of the radiation dose on the lunar surface. *Science Advances*, *6*(39), eaaz1334. https://doi.org/10.1126/sciadv.aaz1334